Research article

QSAR, ADME-Tox, molecular docking and molecular dynamics simulations of novel selective glycine transporter type 1 inhibitors with memory enhancing properties

Mohamed El fadili [a,*], Mohammed Er-rajy [a], Hamada Imtara [b], Omar M. Noman [c], Ramzi A. Mothana [c], Sheaf Abdullah [d], Sara Zerougui [a], Menana Elhallaoui [a]

[a] LIMAS Laboratory, Faculty of Sciences Dhar El Mehraz, Sidi Mohammed Ben Abdellah University, BP 1796 Atlas, Fez 30000, Morocco
[b] Faculty of Arts and Sciences, Arab American University Palestine, Jenin BP Box 240, Palestine
[c] Department of Pharmacognosy, College of Pharmacy, King Saud University, Riyadh 11451, Saudi Arabia
[d] Department of Hand Surgery and Microsurgery, University Medicine Greifswald, Greifswald, Germany

ARTICLE INFO

ABSTRACT

A structural class of forty glycine transporter type 1 (GlyT1) inhibitors, was examined using molecular modeling techniques. The quantitative structure-activity relationships (QSAR) technology confirmed that human GlyT1 activity is strongly and significantly affected by constitutional, geometrical, physicochemical and topological descriptors. ADME-Tox in-silico pharmacokinetics revealed that L28 and L30 ligands were predicted as non-toxic inhibitors with a good ADME profile and the highest probability to penetrate the central nervous system (CNS). Molecular docking results indicated that the predicted inhibitors block GlyT1, reacting specifically with Phe319, Phe325, Tyr123, Tyr 124, Arg52, Asp475, Ala117, Ala479, Ile116 and Ile483 amino acids of the dopamine transporter (DAT) membrane protein. These results were qualified and strengthened using molecular dynamics (MD) study, which affirmed that the established intermolecular interactions for (L28, L30–DAT protein) complexes remain perfectly stable along 50 ns of MD simulation time. Therefore, they could be strongly recommended as therapeutics in medicine to improve memory performance.

1. Introduction

About 25% of the worldwide population suffers from neurological disorders, according to the World Health Organization (WHO) report, published in 2001 [1]. Many of these neurological diseases are the result of memory dysfunctions [2]. The present work aims to discover successful candidate drugs that can improve memory performance. To achieve this objective, we have processed with the assistance of molecular modeling techniques, a set of forty pyrrolo [3,4-c]pyrazole and azetidine-based analogs, acting as selective glycine transporter type 1 (GlyT1) inhibitors, considering that GluT1 is one of the most essential neurotransmitters that control learning and memory functions [3,4].

Over the last decade, the glycine transporter type 1 (GlyT1) has received enormous interest as it is one of the key constituents of glycine metabolism in the central nervous system (CNS). Whereas, the amino acid glycine is an excitatory and inhibitory

---

* Corresponding author.
E-mail address: Mohamed.elfadili@usmba.ac.ma (M. El fadili).

neurotransmitter in the vertebrate central nervous system. In the cortex, hippocampus, and thalamus areas, glycine regulates excitatory neurotransmission as a mandatory co-agonist at *N*-methyl-D-aspartate (NMDA) receptors (glycine B sites). Inversely, it acts as an inhibitory neurotransmitter at strychnine-sensitive glycine receptor ion channels (glycine A sites) mainly present in the brainstem, cerebellum, and spinal cord [3,5]. Hence, GlyT1 inhibitors have been introduced into the clinic as potent treatments for obsessive-compulsive disorder (OCD), negative and cognitive symptoms associated with schizophrenia, addiction, depression, and Parkinson's disease [3,5,6]. Nowadays, computer-assisted drug design (CADD) based on in silico techniques has gained enormous importance and has been widely reported in the literature. In this regard, we examined all 40 GlyT1 inhibitors, through the use of CADD technology, to detect and identify non-toxic, highly effective CNS drug candidates, that will be able to produce highly stable chemical bonds between these candidate inhibitors of glycine transporter and the membrane protein of drosophila melanogaster dopamine transporter (DAT), which would be intended to treat memory impairments [7].

In the first stage, we started this task, using quantitative structure-activity relationships (QSAR) as a technique largely applied in the field of drug discovery, predicting the human GlyT1 activity of 40 pyrrolo [3,4-c]pyrazole and azetidine derivatives, based on two mathematical QSAR models, which were established thanks to the use of multiple linear regression (MLR) and multiple non-linear regression (MNLR) respectively, to model the linear and nonlinear relationships between human GlyT1 activity and different types of molecular descriptors [6,8].

In the second part, we have predicted adsorption, distribution, metabolism, excretion, and toxicity (ADMET) properties for forty selective inhibitors of glycine transporter type 1, with the aim of discovering qualified drugs with a favorable ADMET profile [9,10]. Subsequently, we have performed the molecular docking study for the predicted ligands that traverse the central nervous system, to identify the established intermolecular interactions towards the amino acids from DAT protein encoded as 4M48. pdb [11,12].

Lastly, this work has been concluded using molecular dynamics simulations during 50 ns, to verify the stability of (predicted ligands-protein target) complexes, and monitoring the total free energy variation in Kcal/mol of each complex based on the MM-GBSA approach [6,13,14].

2. Materials and methods

2.1. Experimental database

The current study includes forty pyrrolo [3,4-c]pyrazole and azetidine-based derivatives (Fig. S1) having human GlyT1 activities [3,5], that were subsequently expressed on a logarithmic decimal scale ($pIC_{50} = - \log_{10} IC_{50}$), as presented in Table S1.

2.2. Molecular descriptors calculation

To model the quantitative structure-activity relationships (QSAR), various types of molecular descriptors have been calculated as presented in Table S2. With the help of Gaussian 09 software [15], we have calculated the quantum descriptors, to optimize the 3D geometries and ensure molecular stability with minimized energies using the density functional theory (DFT) coupled with B3LYP/6-31 + G (d,p) basis [16,17]. Then, we executed the thermodynamic, topological, and physicochemical descriptors based on the MM2 technique using the ChemBio3D software [18]. Finally, the constitutional descriptors have been processed through the ACD/chemsketch software [19].

2.3. Statistical methods

To minimize the size of the molecular descriptors into a reduced number of factorial axes (or principal components), we have applied the principal component analysis (PCA), as a very important step to identify the most predictive variables that can influence the biological activity of inhibitors [20]. Thereafter, two statistical methods were performed on the training set (N = 32) to develop a predictive QSAR model using XLSTAT 2014 software [21]. The first one is the multiple linear regression (MLR) technique, which is widely used to investigate the linear relationship between the biological activity of pIC_{50} order and the previously calculated molecular descriptors. The second, is the multiple non-linear regression (MNLR) analysis, which is adapted to examine the nonlinear relationship established between the inhibitory activity and the calculated descriptors [22]. Next, the MNLR and MLR QSAR models were checked with external validation for a test set (N = 8) and further evaluated with internal validation using the leave-one-out (LOO) procedure of the cross-validation (CV) technique. Additionally, the Tropsha and Golbreikh criteria, applicability domain, and the Y-randomization test were also utilized to evaluate the predictive potential and robustness of the developed QSAR models [23,24].

2.4. In silico pharmacokinetics, drug-likeliness, and ADMET depiction exploration

To obtain a novel medication with high efficiency and less experimental investigation time, it's mandatory to evaluate their absorption, distribution, metabolism, excretion, and toxicity (ADMET) properties in the human organism before beginning any clinical trials, verifying the five rules of Lipinski [25], and respecting the Veber, Ghose, Egan and Muegge violations number of drug candidates [26–30]. For this purpose, we have predicted in silico pharmacokinetics and ADMET properties of the candidate's molecules as GlyT1 inhibitors enhancing memory performance, using pkCSM and online SwissADME servers, respectively [31,32].

2.5. Molecular docking simulation

Molecular docking is an accurate, quick, and successful technology in the field of drug discovery [33]. It is largely applied to examine the intermolecular interactions established between the candidate drug and the targeted protein. For this goal, we have extracted the 3D coordinates of the drosophila melanogaster dopamine transporter encoded as 4M48 from the data bank of proteins (pdb) [34], with a resolution equal to 2.96 Å, using the X-ray diffraction method [35]. With the assistance of the Discovery Studio 2021 (BIOVIA) software package [36], we have deleted the water molecules (H_2O) and suspended ligands that were bound to the protein, such as nortriptyline ($C_{19}H_{21}N$), cholesterol ($C_{27}H_{46}O$), chloride and sodium ions (Na+, Cl-). Then, we added the polar hydrogens, to ensure that the performance of the cavity method is improved [37]. Thereafter, we launched the prepared protein, L28, and L30 ligands in AutoDock 4.2 software [38], going from PDB to PDBQT format. With the assistance of the AUTOGRID algorithm, the grid box dimensions were fixed on (−42.56 Å, −0.46 Å, −55.07 Å), choosing the 3D-structure sizes on (110, 110, 110) with a spacing of 0.375 Å, and running ten genetic algorithms for twenty-five million evals. Lastly, 3D and 2D intermolecular interactions of candidate drug-targeted protein complexes were visualized with the help of Discovery Studio 2021 (BIOVIA) software [36,37].

2.6. Molecular dynamic

To ensure the intermolecular interactions stability of protein-ligand complexes, we have performed the molecular dynamics technique during 50 ns using Desmond software, a package of Schrödinger LLC [39]. The output files of molecular docking were defined as input files of molecular dynamic simulations, which were prepared by Protein Preparation Maestro, which optimizes and minimizes the pre-treated complexes in the System Builder utilizing a solvent model having an orthorhombic box of transferable intermolecular interaction potential 3 points (TIP3P) type, and an OPLS-like force field [40]. In addition, the models were neutralized with the insertion of water molecules and counter ions, where the physiological conditions were reproduced in 0.15 M salts (Na+, Cl-), under a temperature and pressure of 300 K and 1 atm, respectively. After every 10 ps of evaluation, we recorded the trajectories, and we examined the stability of the simulations, studying the root mean square deviation (RMSD) for each complex. Thereafter, we have supervised the root-mean-square fluctuation (RMSF), polar surface area (PSA), solvent accessible surface area (SASA), gyration radius (Rg), and molecular surface area (MolSA) variations [6]. Lastly, the free energies of the protein-candidate drug interactions were tested at 50 ns of simulations time, with the help of MM-GBSA technology [41].

3. Results and discussion

3.1. Principal component analysis

To minimize the dimension of molecular descriptors in a reduced number of principal components, we have focused on the correlation matrix given by the principal component analysis (PCA) technique, as one of the most applied multivariate analyses [42]. We have started this task with a database of 40 molecules and 40 different descriptors as illustrated in Table S2. Then, we reduced this uncontrollable number of descriptors into 25 uncorrelated descriptors, as the strongly correlated descriptors between them (Pearson correlation coefficient>0.9) were removed, so to facilitate the development of QSAR mathematical models.

3.2. Experimental database

The present study is intended to develop a mathematical QSAR model between the structural descriptors of human GlyT1 inhibitors and their biological activities of pIC_{50} order. For this reason, we have worked on an experimental database of forty compounds and twenty-five uncorrelated descriptors. Then, we based on thousands of randomizations with a 'stepwise' option, dividing our statistical database into training and test sets. The first set contains 80% of global data (32 molecules) taken to establish the QSAR model, and the second set includes 20% (8 molecules) selected to validate the established model [6,37,43].

3.3. Multiple linear regression

The first QSAR model was constructed for a training set of thirty-two molecules (N = 32) using multiple linear regression (MLR) as a statistical method capable to evaluate the linear relationship between the molecular descriptors and the inhibitory activity [44]. The

Table 1
The significant weights of the selected descriptors.

Source	Value	Standard deviation	t	Pr > |t|	Lower terminal (95%)	Higher terminal (95%)
Constante	3.823	1.307	2.926	**0.007**	1.137	6.509
MW	0.010	0.002	5.608	**< 0.0001**	0.007	0.014
NRB	−0.321	0.056	−5.769	**< 0.0001**	−0.436	−0.207
Log P	0.280	0.095	2.950	**0.007**	0.085	0.474
TD	−0.222	0.105	−2.118	**0.044**	−0.437	−0.007
PSA	0.045	0.010	4.453	**0.000**	0.024	0.065

process was based on the best values of the correlation, determination, and adjustment coefficients (R, R^2, and R^2adj). So, the optimal MLR QSAR model was developed in Eq. (1):

$$pIC_{50} = 3.82 + 0.01 \times MW - 0.32 \times NRB + 0.28 \times Log\ P - 0.22 \times TD + 0.045 \times PSA \tag{1}$$

The predictive QSAR model introduces the following selected descriptors: molecular weight (MW), partition coefficient (Log P), number of rotatable bonds (NRB), polar surface area (PSA), and topological diameter (TD), as included in Table S3.

The slope of each selected descriptor has a probability inferior to 5%, as indicated by the significance test in Table 1. So, the selected variables have a significant impact on the activity at a confidence interval of 95%. Molecular weight, partition coefficient, and polar surface area have a positive effect on activity, but the number of rotatable bonds and topological diameter influence it negatively, as illustrated in Fig. 1. Thus, the compound can be highly active if it's defined by a small value of TD and NRB and given by higher values of MW, Log P, and PSA. According to Fisher's statistical test, the null hypothesis (H0) is rejected because the analysis of variance (Anova) proves that the critical value: [$F_{(32, 5)} = 2.51$, $p < 0.0001$] is much smaller than its calculated value ($F = 13.832$), as presented in Table 2. Thus, the dependent variable (pIC_{50}) and the independent variables (5 selected descriptors) are defined by a homogeneous variance. In addition, the correlation, determination, and adjustment coefficients are equal to $R = 0.85$, $R^2 = 0.73$, and $R^2adj = 0.67$, respectively. Which confirms a solid relationship between the inhibitory activity and the molecular descriptors, and a strong predictive performance of the MLR QSAR model, with a minimal root mean square error (RMSE = 0.297). Consequently, we conclude that human GlyT1 activity is strongly and significantly correlated with constitutional (MW), physicochemical (Log P), geometrical (NRB), and topological (PSA and TD) descriptors.

3.4. Multiple non-linear regression

To model the non-linear relationship between the previously selected descriptors and human GlyT1 activity, we have applied the multiple non-linear regression (MNLR) technique [45], for a training set of thirty-two molecules (N = 32) using the following programmed function Eq. (2) [6]:

$$Y = a0 + \sum_{i=1}^{n} \left(ai \times Xi + bi \times Xi^2 \right) \tag{2}$$

Where, Y: is the predicted activity with MNLR QSAR model, a0: is the constant of the mathematical model, Xi: is the selected descriptor, ai and bi: are the slopes of each molecular descriptor for 1 and 2°, respectively [6]. Thus, we have obtained the second QSAR model as presented by Eq. (3):

$$pIC_{50} = -0.487 + 0.006 \times MW - 0.629 \times NRB + 0.577 \times Log\ P - 0.477 \times TD + 0.232 \times PSA + 3.887E\text{-}6 \times MW\text{\textasciicircum}2 + 0.024 \times NRB\text{\textasciicircum}2 - 0.055 \times Log\ P\text{\textasciicircum}2 + 0.010 \times TD\text{\textasciicircum}2 - 0.001 \times PSA\text{\textasciicircum}2 \tag{3}$$

This predictive model is qualified by a strong correlation coefficient of $R = 0.88$, a good determination coefficient ($R^2 = 0.78$) and a low root mean square error ($RMSE = 0.296$).

In conclusion, the MLR and MNLR QSAR models noted in Equations (1) and (3) respectively, affirm that human GlyT1 activity is actually affected by five selected descriptors. Where, the weight of active molecule (MW), its lipophilicity in octanol/water solvent (expressed by the partition coefficient: Log P), and the region of its polar surface area (PSA) have all a positive impact. While, the
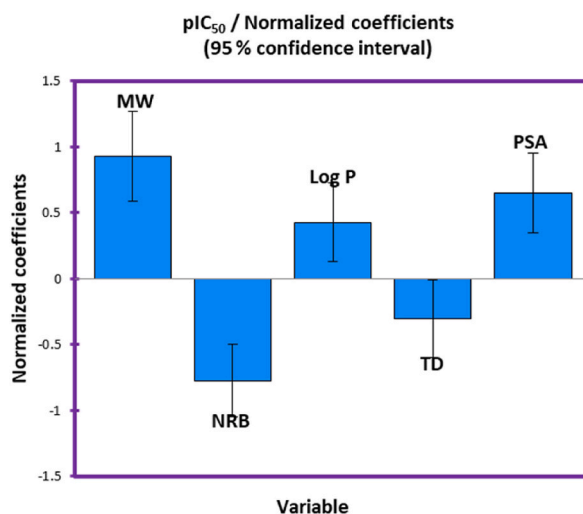
Fig. 1. The impact of molecular descriptors on the biological activity.

Table 2

Analysis of variance using the fisher test.

Source	DDL	Total square	Mean square	F	Pr > F
Model	5	6.086	1.217	**13.832**	<0.0001
Error	26	2.288	0.088		
Adjusted total	31	8.374			

topological diameter (TD) and the number of rotatable bonds (NRP) have a negative effect on GluT1 activity.

3.5. Validation of predictive QSAR models

3.5.1. Applicability domain

To examine the applicability of quantitative activity-structure relationship models, we have performed the applicability domain (AD) technology. Using IBM SPSS Statistics 22 software. Based on William's diagram shown in Fig. 2. The warning leverage ($h^* = 0.56$) was indicated using Eq. (4) [46]:

$$h^* = [3 \times (p + 1) / n], (p = 5, n = 32) \tag{4}$$

Where, p: is the number of selected descriptors. n: is the number of molecules in the training set, and 3: is the absolute value limit of the standardized residuals interval on the Y-axis [47]. We note that all molecules in the training and test sets have a leverage under the critical leverage value, and they are all placed in the confidence interval of [-3, +3], except two molecules (19 and 29) of the test set, which are considered as outliers because they have a standardized residual of -4.601 and -3.785, respectively. So, the QSAR model was correctly predicted, where the outliers were removed and the 38 remaining molecules were successfully examined in the applicability domain [6,43,48].

3.5.2. External validation

To evaluate the reliability of the QSAR predictive model and to ensure its application, it is strictly necessary to validate it on some novel compounds comprised in the test set using the external validation technique [49]. Based on a training test of thirty-two molecules, we have tested six new compounds from the test set and we have obtained the results of predicted activities using the linear and nonlinear regression techniques, as displayed in Table 3.

The first QSAR model, which was developed using the multiple linear regression (MLR) technique, is given by an external validation correlation coefficient equal to $R^2 ext = 0.867$, as presented in Fig. 3, and the second QSAR model, developed by multiple nonlinear regression (MNLR) technique, is defined by an external validation correlation coefficient of $R^2 ext = 0.946$, as illustrated in Fig. 4. Thus, MLR and MNLR QSAR models are externally validated because they are characterized by an external validation correlation coefficient greater than 0.6.

3.5.3. Internal validation

The leave-one-out procedure (LOO) of the cross-validation technique (CV) was performed to validate internally the developed QSAR models. For this purpose, we tested each molecule once, with the development of a new mathematical model on thirty-one
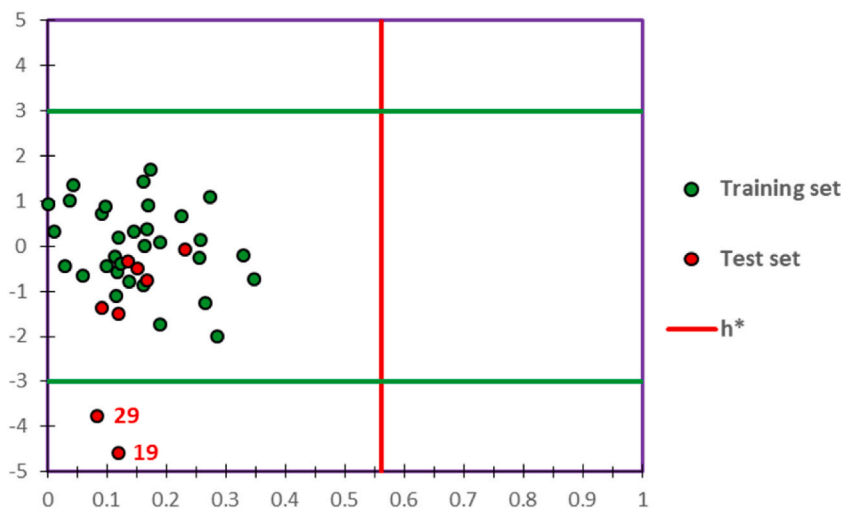
Fig. 2. William's diagram of the predictive QSAR models. (Green and red dots display the molecules of training and test sets, respectively. The red line indicates the warning leverage, and the green lines show the confidence interval of [-3, +3])

Table 3

The observed and predicted activities of pIC$_{50}$ order using MLR and MNLR QSAR models.

Molecules number	Observed pIC$_{50}$	Predicted pIC$_{50}$ (MLR)	Predicted pIC$_{50}$ (MNLR)
4[a]	7.638	8.044	7.897
10[a]	7.796	7.825	7.908
14[a]	8.222	8.323	8.410
17[a]	7.569	8.017	7.954
18[a]	7.921	8.069	8.012
31[a]	6.848	7.076	7.200

[a] Indicates the test set molecules.
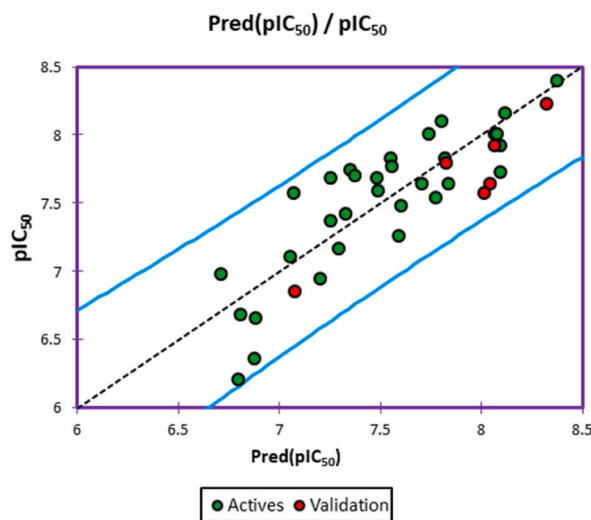
Fig. 3. The correlation among the predicted and observed activities using multiple linear regression. (Green and red dots indicate the molecules in the training and test sets, respectively)
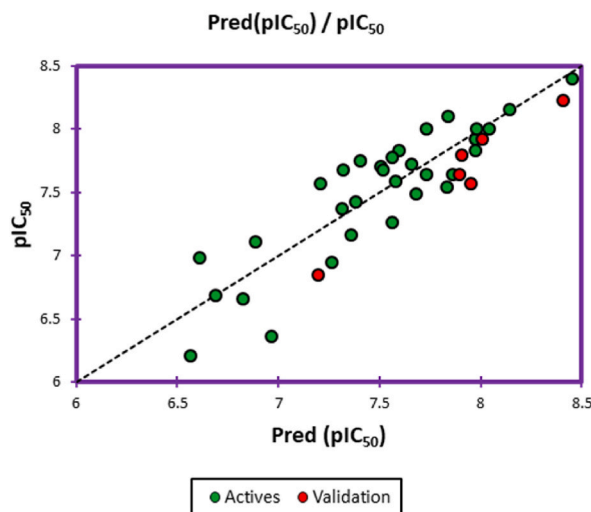
Fig. 4. The correlation among the predicted and observed activities using multiple nonlinear regression. (Green and red dots indicate the molecules in the training and test sets, respectively)

compounds (N-1 = 31) and prediction of the inhibitory activity of this tested molecule [50], as resulted in Table 4, this process was repeated for all training set molecules [46]. Thereafter, we calculated the quadratic coefficient (Q^2 cv) of cross-validation using Eq. (5) [43]:

Table 4
The observed and predicted activities using MLR, MNLR and CVLOO techniques.

Molecules number	Observed pIC$_{50}$	Predicted pIC$_{50}$ (MLR)	Predicted pIC$_{50}$ (MNLR)	Predicted pIC$_{50}$ (CVLOO)
1	7.824	7.551	7.601	7.541
2	8.097	7.802	7.844	7.780
3	7.638	7.836	7.866	7.856
5	7.921	8.097	7.976	8.128
6	7.770	7.559	7.563	7.528
7	7.638	7.709	7.732	7.721
8	8.000	7.743	7.734	7.704
9	7.420	7.329	7.387	7.325
11	8.000	8.067	8.042	8.105
12	8.155	8.119	8.148	8.105
13	8.000	8.081	7.983	8.114
15	8.398	8.376	8.458	8.370
16	7.538	7.775	7.833	7.824
20	7.108	7.056	6.887	7.047
21	7.161	7.298	7.361	7.307
22	7.745	7.351	7.406	7.318
23	6.678	6.813	6.691	6.833
24	6.979	6.712	6.616	6.645
25	6.947	7.205	7.266	7.267
26	7.678	7.258	7.322	7.156
27	6.356	6.878	6.970	7.027
28	7.699	7.376	7.511	7.233
30	7.260	7.592	7.562	7.650
32	7.481	7.602	7.684	7.625
33	7.678	7.485	7.522	7.418
34	7.721	8.098	7.660	8.259
35	7.569	7.073	7.208	6.944
36	6.201	6.797	6.569	7.075
37	6.658	6.882	6.825	7.019
38	7.367	7.257	7.316	7.230
39	7.585	7.493	7.580	7.473
40	7.824	7.823	7.973	7.823

$$Q^2cv = 1 - \frac{\sum\limits_{i}^{n}(Yobs - Ypred)^2}{\sum\limits_{i}^{n}(Yobs - Ymean)^2} \tag{5}$$

Where, *Yobs*: signifies the observed activity, *Ypred*: is the predicted activity, and *Ymean*: presents the average of the observed activities. Although the obtained value of quadratic coefficient ($Q^2cv = 0.55$) is higher than 0.5, the established QSAR model is robust, reliable, and has a stronger internal predictivity.

3.5.4. Validation using Y-randomization test

Golbraikh and Tropsha's study argues that the internal predictive accuracy of the quantitative structure-activity relationships (QSAR) model, explained by a large value of the quadratic coefficient of leave one out cross-validation (CVLOO), has a tendency to be overestimated and may be the result of a lucky correlation. For this reason, the Y-Randomization test is necessary [6,51]. With the assistance of java Platform SE binary, we have tested the quality of the established QSAR model running 100 randomizations as

Table 5
Tropsha and Golbraikh conditions to examine the accuracy of generated MLR QSAR model.

Parameter	Equation	Model score	Threshold	Comment
R^2	$R^2 = 1 - \frac{\sum(Yobs - Y\,cal)^2}{\sum(Yobs - \overline{Yobs})^2}$	0.73	>0.6	Accepted
$R^2 adj$	$R^2 adj = \frac{(N-1)R^2 - p}{N - p - 1}$	0.67	>0.6	Accepted
$R^2 test$	$R^2\,test = 1 - \frac{\sum(Ycal(test) - Y\,obs(test))^2}{\sum(Yobs(test) - Y\,obs(train))^2}$	0.87	>0.6	Accepted
$Q^2 cv$	$Q^2 cv = 1 - \frac{\sum(Ycal - Y\,obs)^2}{\sum(Yobs - \overline{Yobs})^2}$	0.55	>0.5	Accepted
$R^2 rand$	Average of the 100 $R^2 rand\,(i)$	0.16	$< R^2$	Accepted
$Q^2 cv$ 'LOO' rand	Average of the 100 $Q^2 cv$ 'LOO' rand (i)	−0.30	$< Q^2 cv$	Accepted
$cR^2 p$	$cR^2 p = R \times \sqrt{R^2 - (Average\ R_{rabd})^2}$	0.65	>0.5	Accepted

resulted in Table S4. The results of the Y-Randomization test indicate that the value of the cR^2p criteria is 0.65, which is greater than 0.5. Additionally, the values of correlation, determination, and cross-validation with the leave-one-out procedure coefficients of the original model are so much higher than the resulting values for all one hundred randomizations. As a consequence, the human GlyT1 activities as predicted by the originally designed model are not due to random chance [6].

3.5.5. Statistical criteria of golbreikh and Tropsha's study

The predictive MLR QSAR model given in Equation (1), successfully meets the postulated threshold conditions of Tropsha and Golbraikh's theory, as illustrated in the following Table 5.

3.6. In silico pharmacokinetics ADMET prediction

In the beginning, we predicted the human GlyT1 inhibitors using BOILED-Egg as an accurate predictive model, very practical in medicinal chemistry to discover the candidate drugs as presented in Fig. 5. We have noted that 28 and 30 molecules in blue are part of the yellow Egan-egg, so they are predicted as inhibitors with the greatest ability to cross the blood-brain barrier (BBB) and predicted to be effluated from the central nervous system (CNS) by the *P*-glycoprotein. Thus, 24 molecules and the nortriptyline as a co-crystallized ligand bound to the membrane protein of dopamine transporter (DAT), as colored in red, are also part of yellow Egan-egg, but they are predicted not to be effluated from the central nervous system (CNS) by the *P*-glycoprotein. In contrast, the compounds that are part of the white Egan-egg, are predicted as molecules passively absorbed by the gastrointestinal tract [52]. At the second stage, we have predicted the nortriptyline as a co-crystallized ligand compared to 28 and 30 inhibitors which are considered as candidate inhibitors able to penetrate the blood-brain barrier (BBB) and evacuated from the central nervous system (CNS) by the *P*-glycoprotein in the basis of Lipinski, Egan, Veber, Ghose, and Muegge rules, as shown in Table 6. Thus, we have noted that these candidate drugs respect all Lipinski rules like as: MW ≤ 500, 40≤ MR ≤ 130, NRB<10, Log P$_{(octanol/water)}$ < 5, HBA≤10, and HBD<5 [43]. Additionally, they satisfy Veber, Egan, Ghose, and Muegge regulations [53]. In the last step, we studied the pharmacokinetic properties of adsorption, distribution, metabolism, excretion, and toxicity (ADME-Tox) of the candidate molecules. Which were compared to the obtained results for nortriptyline, as resulted in Table 7. We have noticed that L28 and L30 ligands have an excellent human intestinal absorption (HIA superior than 96%), good distribution because they are defined by the human distribution volumes higher than −0.44 Log L/kg, and characterized by a BBB and CNC permeability values greater than −1 Log BB and included in (−2 to −3) Log PS, respectively. So, they are well permeable to the blood-brain barrier (BBB) and the central nervous system (CNS). Moreover, they are all predicted as potent inhibitors of 2C9, 2C19 and 3A4 cytochromes. Then, they present a total clearance of 0.563 and 0.711 Log ml/min/kg respectively, without any toxicity on the human body. Therefore, we have concluded that L28 and L30 ligands are successfully predicted as not toxic inhibitors of 2C9, 2C19, and 3A4 cytochromes, respecting Lipinski, Veber, Egan, Ghose, and Muegge rules, and they are estimated to penetrate the blood-brain barrier (BBB) with the highest probability. So, they are designed as powerful central nervous system (CNS) agents.
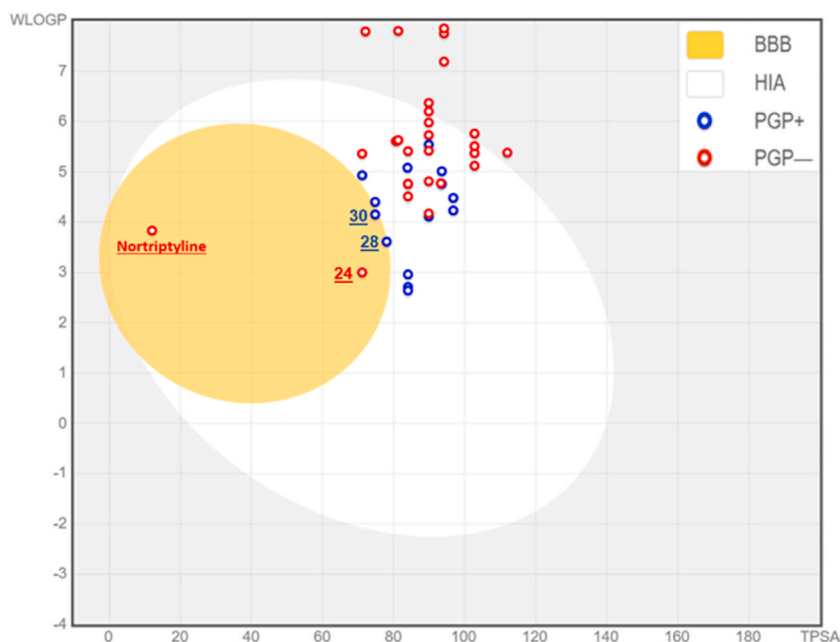
Fig. 5. BOILED-Egg model of nortriptyline and forty pyrrolo [3,4-c]pyrazole and azetidine derivatives. (BBB: blood-brain barrier; HIA: human intestinal absorption; PGP: *P*-glycoprotein).

Table 6

Prediction of physico-chemical parameters of L28, L30, and nortriptyline ligands based on Lipinski, Egan, Veber, Ghose, and Muegge regulations.

Ligands number	Physical and chemical properties						Lipinski violations	Veber violations	Egan violations	Ghose violations	Muegge violations
	Molecular weight (g/mol)	Molar refractive index	Rotatable bonds Number	Log P (Octanol/Water)	Hydrogen Bond acceptors	H-bond donors Number					
Threshold	MW ≤ 500	40≤ MR ≤ 130	<10	<5	≤10	<5	Yes/No	Yes/No	Yes/No	Yes/No	Yes/No
L28	448.47	124.97	4	3.35	6	0	Yes	Yes	Yes	Yes	Yes
L30	423.44	120.78	4	3.23	5	0	Yes	Yes	Yes	Yes	Yes
Nortriptyline	263.38	86.06	3	3.22	1	1	Yes	Yes	Yes	Yes	No

Table 7

ADMET-Tox pharmacokinetic properties of L28, L30, and Nortriptyline ligands.

Ligands number	Absorption	Distribution			Metabolism								Excretion	Toxicity
	Intestinal Absorption (human)	VDss (human)	BBB permeability	CNS permeability	Substrate		Inhibitor						Total Clearance	AMES toxicity
					CYP									
					2D6	3A4	1A2	2C19	2C9	2D6	3A4		
	Numeric (% Absorbed)	Numeric (Log L/kg)	Numeric (Log BB)	Numeric (Log PS)	Categorical (Yes/No)								Numeric (Log ml/min/kg)	Categorical (Yes/No)
L28	96.007	0.234	−0.818	−2.839	No	Yes	No	Yes	Yes	No	Yes	0.563	Not toxic
L30	98.673	0.219	−0.353	−1.865	No	Yes	Yes	Yes	Yes	No	Yes	0.711	Not toxic
Nortriptyline	97.482	1.575	0.808	−1.196	No	Yes	Yes	No	No	Yes	No	0.929	Not toxic

3.7. Molecular docking

Although L28 and L30 ligands are engineered as potent inhibitors with a favorable ADMET profile, thus we have studied their intermolecular interactions towards the drosophila melanogaster dopamine transporter (DAT) of 4M48. pdb code, as a transmembrane protein able to extract the neurotransmitter dopamine out of the synaptic cleft and transfer it into the cytosol of neighboring cells [6, 54–56]. The molecular docking simulations of (L28, L30-protein) complexes were done in the active sites of tricyclic antidepressant nortriptyline (as co-crystallized ligand linked to the targeted protein in his A-chain) which resulted from the ProteinsPlus online server [57], like Tyr124 A, Phe325 A, and Phe43 A amino acids, as presented in Fig. 6.

The molecular docking results presented in Fig. 7, indicate that L28 and L30 ligands have several common intermolecular interactions such as: Two stacked Pi-Pi chemical bonds, established between Phe325 and Phe319 amino acids of the targeted protein and the candidate drugs. A common Pi-Sigma chemical bond was formed between the candidate drugs and Ile116 amino acid with a nuclear distance of 5.91 Å. Three Pi-Alkyl chemical bonds were produced with Ala479, Ile483, and Ala117 amino acids of the responsible protein. A common bond of attractive charge with the nitrogen atom was created with Asp475 amino acid. Additionally, we note that the L28 ligand formed at 6.44 Å a bond of Alkyl type towards Tyr124 amino acid. And created for each one of its two fluorine atoms, a hydrogen bond with Tyr123 amino acid, rendering the L28-protein complex more stable. Also, the L30-protein complex was stabilized via the formation of a hydrogen bond between the candidate drug and the Arg52 amino acid of the targeted protein. Therefore, we conclude that Phe325, Phe319, Ile116, Ala479, Ile483, Ala117, Asp475, Tyr124, Tyr123, and Arg52 amino acids are the responsible sites of human glycine transporter type one (GLUT1) inhibitory activities to improve memory performance.

3.8. Docking validation protocol

The efficiency and accuracy of the molecular docking algorithms were examined through the re-docking method, based on the superposition of the co-crystallized ligand on the docked nortriptyline ligand. The overlay results shown in Fig. 8C, reflects a root mean square deviation (RMSD) of 0.552 Å, which is inferior than 2 Å, so the prediction pose is precise and accurate. In addition, 2D and 3D intermolecular interactions, successively presented in Fig. 8A and B, reveal that docked nortriptyline ligand of cyan color, reacts to Tyr124 and Phe43 amino acids, which are the same sites as those experimentally produced. As a result, the docking validation protocol was successfully examined [6,37,58].

3.9. Molecular dynamic simulation

To examine the stability of intermolecular interactions, produced between L28 and L30 candidate drugs and the targeted protein encoded as 4M48. pdb, we have performed the molecular dynamics simulations of these two complexes during 50 ns [6,14].

The results of dynamic conformational changes of (the L28-DAT protein) complex shown in Fig. 9A, illustrate that protein root
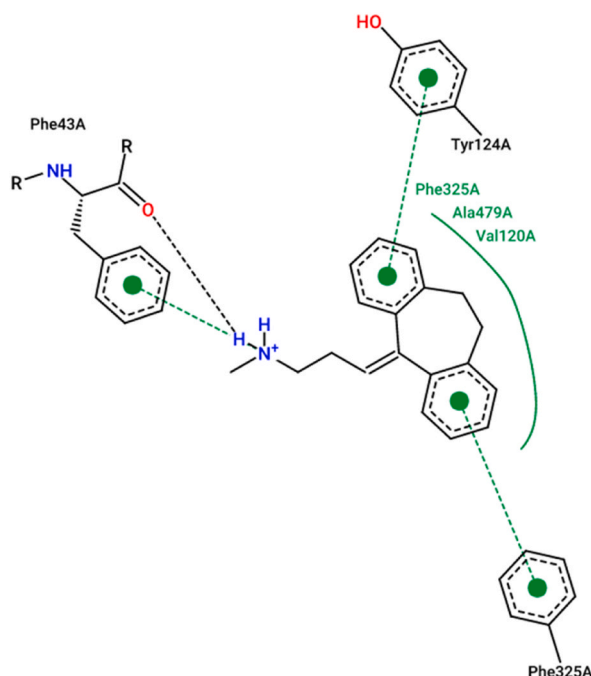
Fig. 6. The active sites of co-crystalized ligand bound to 4M48. pdb protein in A-chain.

L28-DAT protein complex

L30-DAT protein complex

Interactions

🟩 van der Waals		🟥 Pi-Pi Stacked	
🟧 Attractive Charge		🩷 Alkyl	
🟩 Conventional Hydrogen Bond		🩷 Pi-Alkyl	
🟪 Pi-Sigma		🟦 Halogen (Fluorine)	

Donor

Acceptor
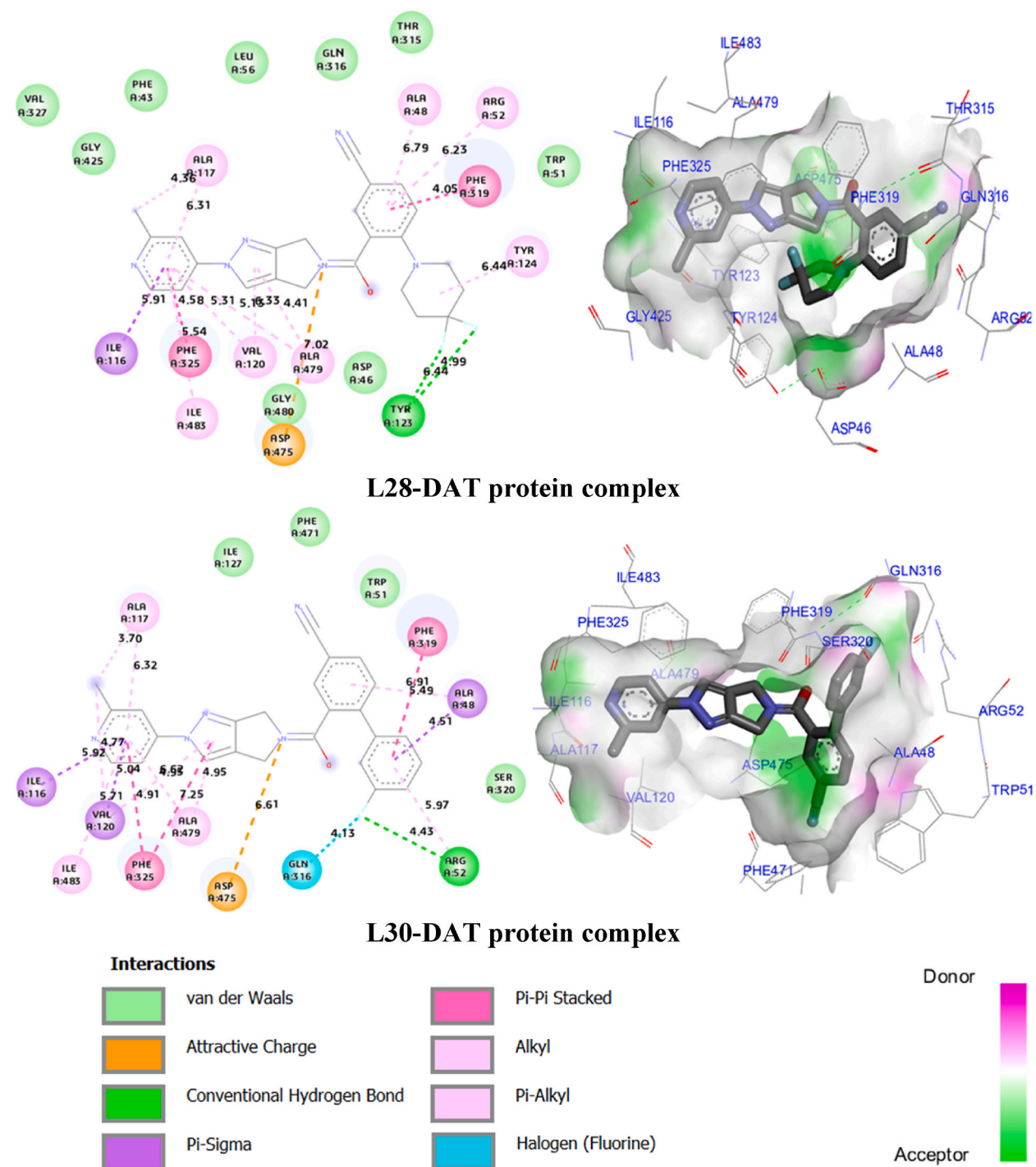
Fig. 7. 2D (left) and 3D (right) inter-molecular interactions, produced between L28 and L30 ligands and DAT protein of 4M48. pdb code with binding energies of −8.72 kcal/mol and −8.70 kcal/mol, respectively. (The left colored rectangles show all types of intermolecular interactions, produced between the candidate ligands and the target protein, while the right key show the donor and acceptor effects in the studied complexes).

mean square deviation (RMSD) in the left Y-axis. Fluctuates around the mean thermal structure during 50 ns of simulation time, because deviation changes in the range of 1–3 Å are acceptable for small globular proteins. Thus, the simulation was well-balanced. In addition, the evolution of the ligand RMSD in the right Y-axis through the heavy atoms, reveals the ligand stability with respect to the protein targets, when the studied complex was first aligned with the reference protein backbone, as the observed values of ligand RMSDs are nearly the same as the protein RMSDs values. Thus, the ligand had not diffused away of its primary binding site. Moreover,
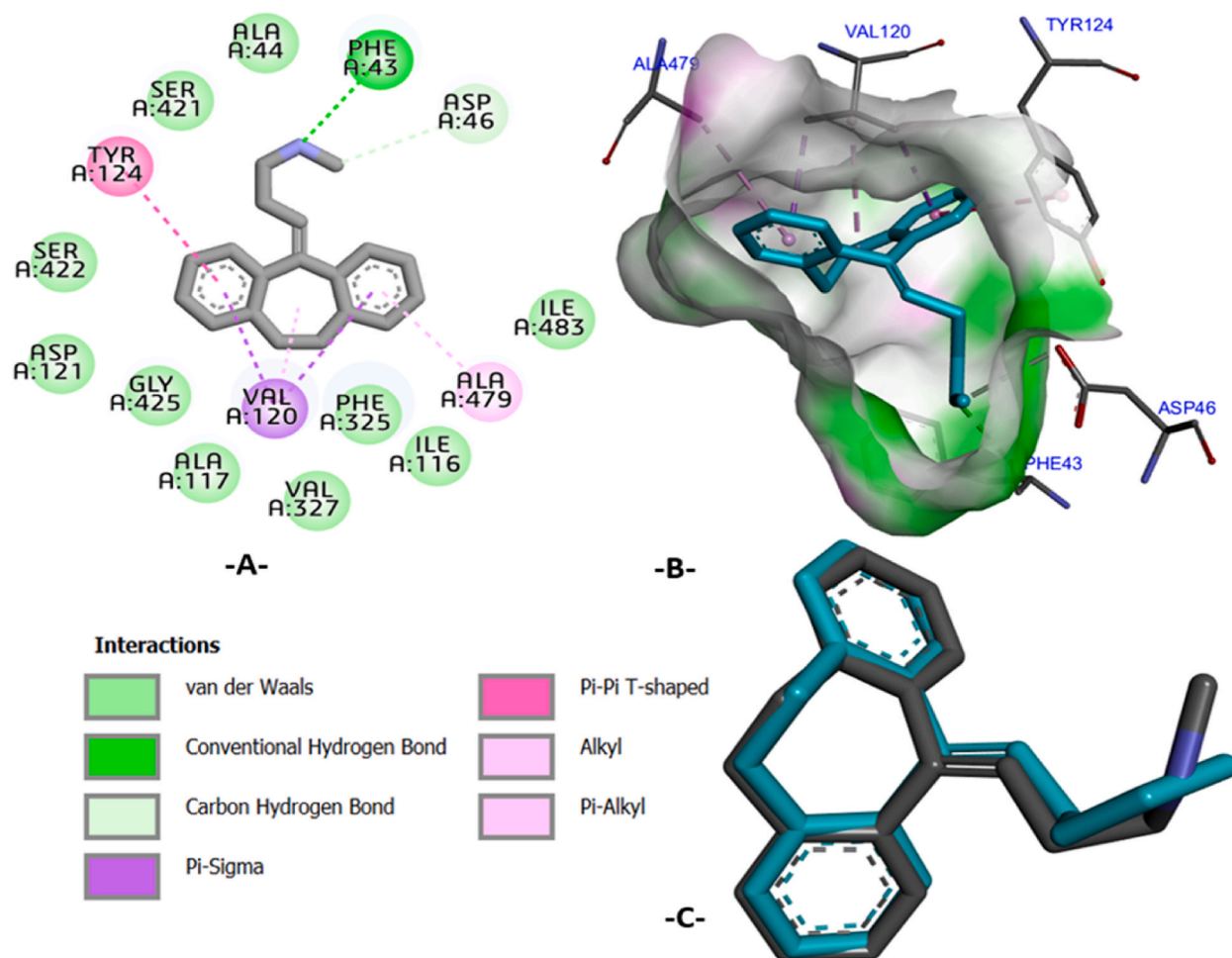
Fig. 8. 2D (A) and 3D (B) visualization of intermolecular interactions created between the docked nortriptyline and 4M48. pdb protein with a binding energy of −8.36 kcal/mol, and re-docking pose (c) defined by a RMSD value of 0.552 Å (docked nortriptyline in cyan and co-crystallized nortriptyline colored by the atomic elements). (The key-colored rectangles show all types of intermolecular interactions, produced between the nortriptyline and the target protein)

the evolution of the root mean square fluctuation (RMSF) was also controlled to investigate the influence of ligand binding on the internal dynamics of DAT protein over 50 ns, in which *C*- and *N*-terminal tails tend to fluctuate more than any other protein part. Similarly, alpha helices and beta strands as secondary structure elements are generally more rigorously rigid than the non-structured protein part, so they fluctuate considerably less than the buckle regions. Just one oscillation of 3.7 Å, has been detected in the buckle region of the residue 390. In contrast, all other fluctuations were inferior to 3 Å, as noted in Fig. 9B, which indicates the absence of a conformational change of the protein caused by its binding towards the ligand, and the stability of the produced complex. The values of gyration radiuses (*r*-Gyr) have oscillated in a relatively short range of 4.40–5.35 Å along the simulation time, as noticed in Fig. 9C, which reveals a few conformational changes in the compactness of the L28 ligand, so the DAT protein has an acceptable flexibility after being bound to the candidate drug. Also, the evolution of solvent accessible surface area (SASA), was done to evaluate the solvent accessibility of (L28-DAT protein) complex over 50 ns of simulation time, as we have recorded a minimal oscillation, included between 20 and 90 Å^2, which demonstrates that the drug structure was approximately unchanged during the simulation process. Moreover, the molecular surface area (MolSA) associated with a Van Der Waals surface was calculated with a probe radius of 1.4 Å, has been fluctuated between 400 and 430 Å^2. Furthermore, we have noticed that the polar surface area (PSA) which is mainly influenced by nitrogen and oxygen atoms, changes between 75 and 145 Å^2, with some very small maximum and minimum fluctuations. Eventually, the graph of total energy, obtained using the MM-GBSA approach, displays some minimal oscillations around the mean of −58.360388 kcal.mol-1, which are progressively stabilized from 25 ns until the end of the simulation as displayed in Fig. 9D.

Regarding the second complex, we noticed that the DAT protein was also characterized by a root mean square deviation (RMSD) included between 1 and 3 Å, where the observed values of the ligand RMSD oscillate in parallel with those of the protein RMSD, as presented in Fig. 10A. So, the simulation was well equilibrated for the (L30-DAT protein) complex, and the candidate drug had not diffused away from its primary link site. Additionally, the graph of root mean square fluctuations (RMSFs), indicates only two
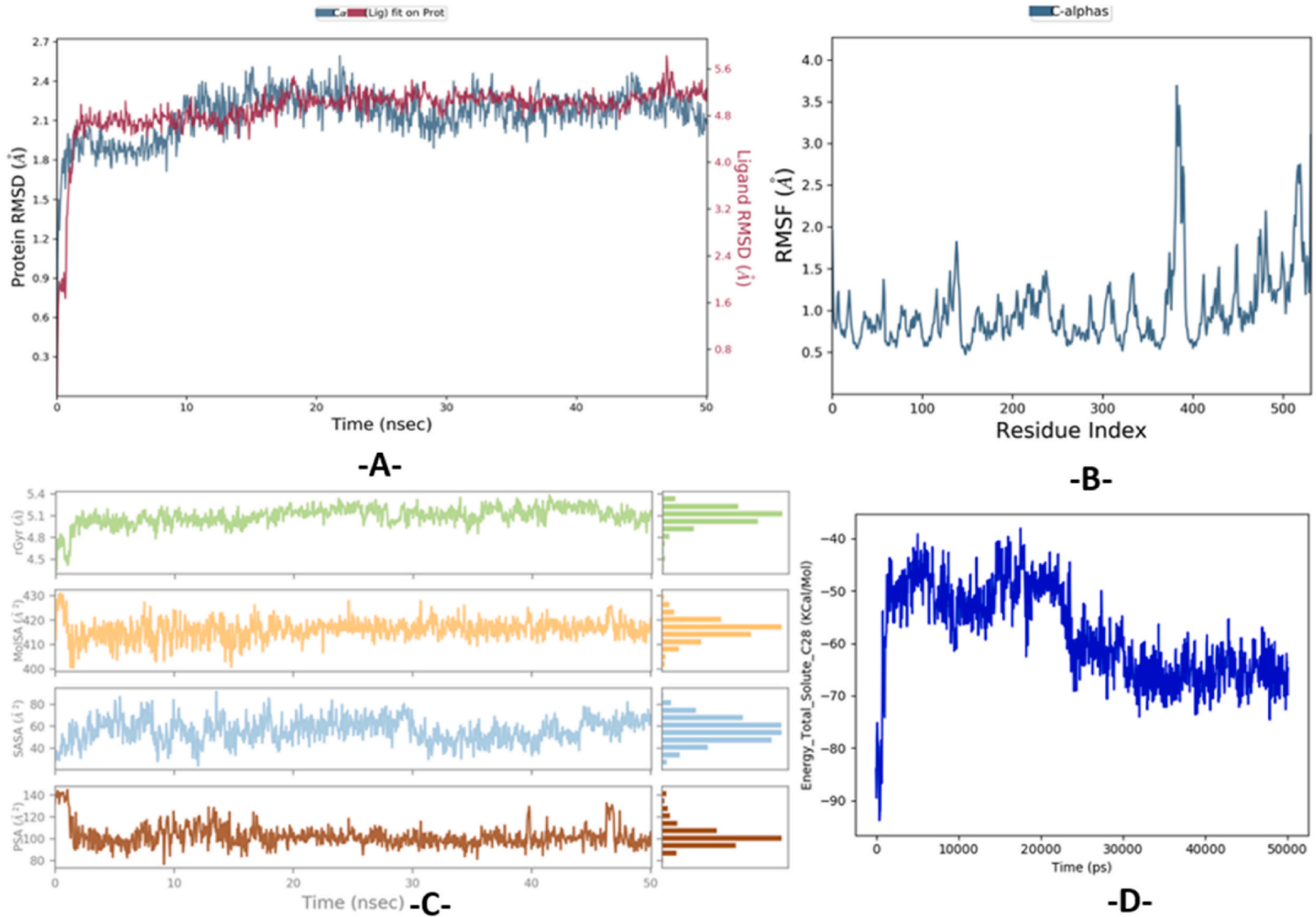
Fig. 9. Evolution of RMSD, RMSF, Rg, MolSA, SASA, PSA and total free energy during 50 ns, for (L28-DAT protein) complex.
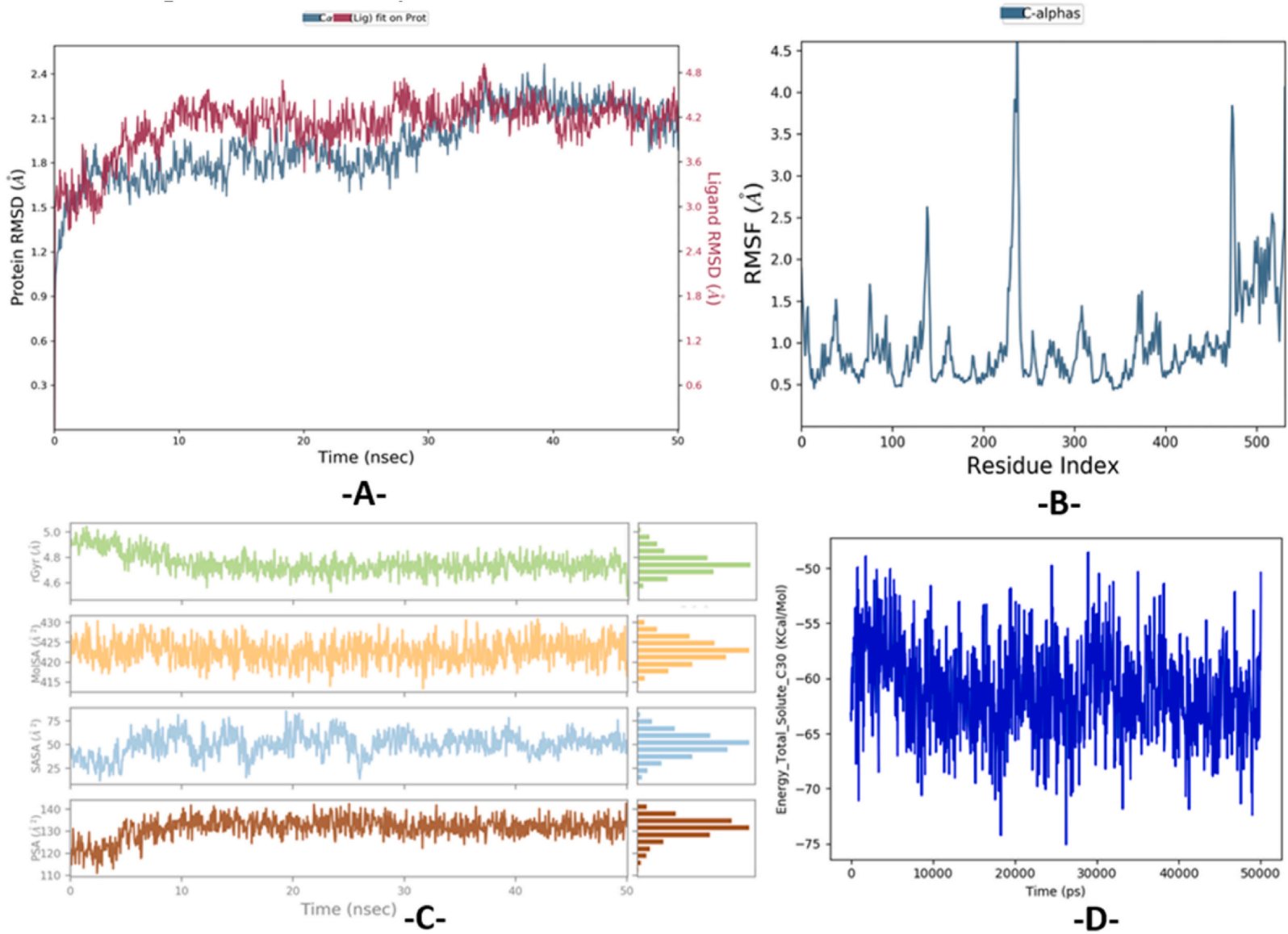
Fig. 10. Evolution of RMSD, RMSF, Rg, MolSA, SASA, PSA, and total free energy during 50 ns, for (L30-DAT protein) complex.
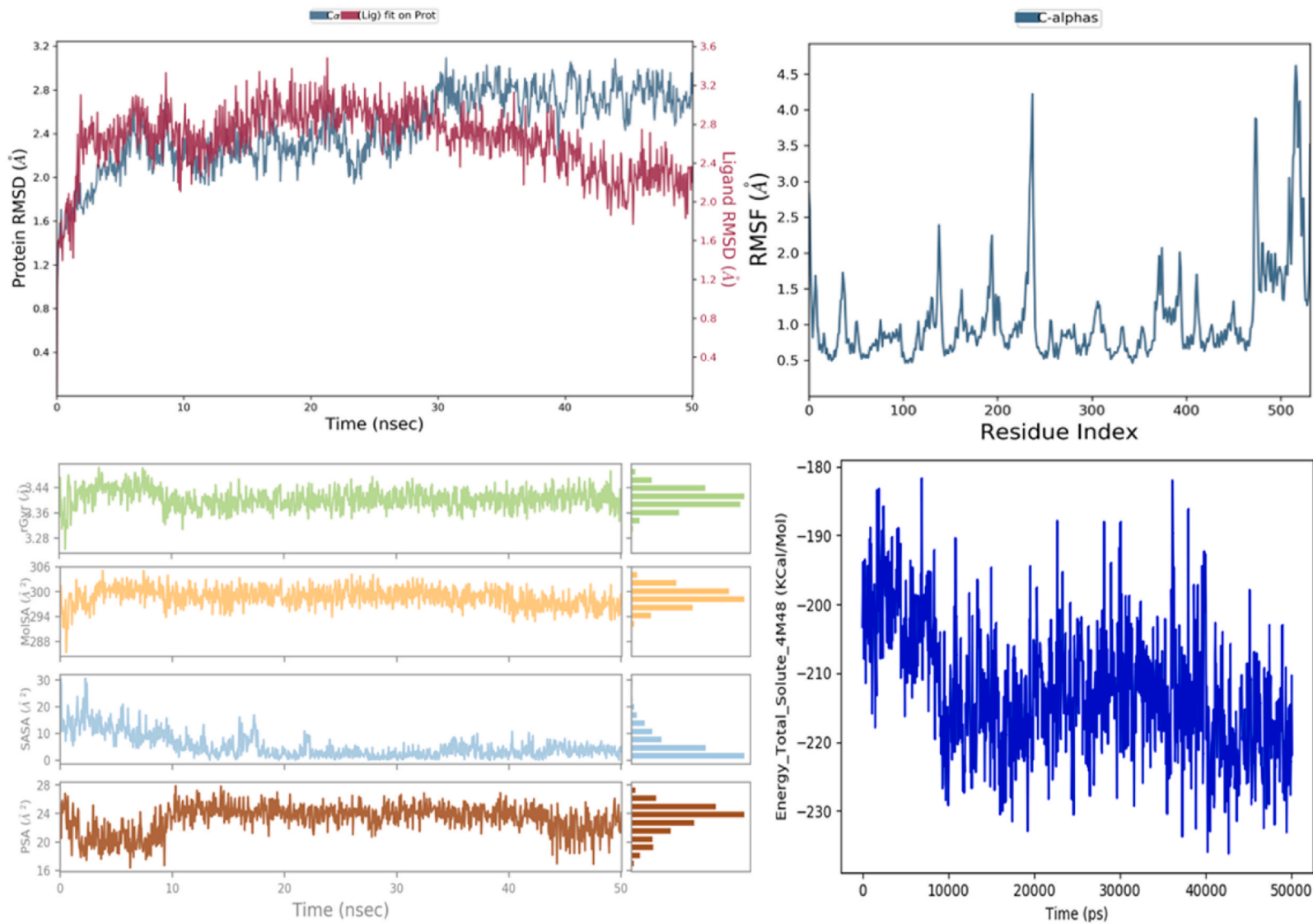
Fig. 11. Evolution of RMSD, RMSF, Rg, MolSA, SASA, PSA, and total free energy during 50 ns, for (Nortriptyline -DAT protein) complex.

fluctuations greater than 3 Å. The first one was recorded at 4.6 Å for residue 230, and the second one was detected at 4.7 Å for residue 480, as shown in Fig. 10B, indicating that the DAT protein binds to the drug with extremely small conformational changes. Subsequently, we have monitored the evolution of gyration radiuses (r-Gyr), solvent accessible surface area (SASA), molecular surface area (MolSA), and polar surface area (PSA) properties, which are generally subject to very small fluctuations as displayed in Fig. 10C. So, the drug structure remained approximately unchanged during 50 ns of simulation time, and the DAT protein has an agreeable flexibility during its interaction with the L30 candidate drug. Finally, the total energy graph of the (L30-DAT protein) complex, given with the assistance of the MM-GBSA approach, displays slight fluctuations about the mean of -61.193294 kcal.mol-1, as shown in Fig. 10D, which means that the complex remains very stable over the simulation time.

Consequently, we conclude that intermolecular interactions produced in the (DAT protein-L28, and L30 ligands) complexes are dynamically more stable because their studied properties remained in equilibrium throughout the MD simulation. Moreover, they present similar stability compared to MD calculations of nortriptyline as a positive control molecule crystallized to the DAT protein complex. Where the RMSD values do exceed not 3 Å, and RMSF values display just negligible fluctuations. Furthermore, the variation of free energies obtained with the use of MM-GBSA approach remains stable during the molecular dynamics simulation time, as displayed in Fig. 11.

4. Conclusion

An in silico investigation was performed for forty pyrrolo [3,4-c]pyrazole and azetidine-based derivatives, to discover an effective drug for enhancing human memory performance. In the beginning, two predictive QSAR models were developed using MNLR and MLR techniques and were successfully validated by internal and external validation, Y-randomization test, applicability domain, Tropsha, and Golbreikh criteria, indicating that MW, Log P, NRB, PSA, and TD descriptors have a key function in the human glycine transporter type one (GlyT1) activity. Afterward, a pharmacoinformatic-based approach revealed that L28 and L30 ligands were predicted as non-toxic inhibitors of 2C9, 2C19, and 3A4 cytochromes, with a desirable ADMET profile, meeting the rules of Lipinski, Egan Veber, Muegge, and Ghose. So, they are designed as candidate drugs, most likely to penetrate the central nervous system (CNS). For this reason, they were specially selected for molecular docking simulation, which revealed that they react with Phe319, Phe325, Tyr123, Tyr 124, Arg52, Asp475, Ala117, Ala479, Ile116, and Ile483 amino acids of a membrane protein from the dopamine transporter (DAT) of 4M48. pdb code. Finally, the stability of intermolecular interactions produced between the candidate drugs and the targeted protein was successfully examined through the molecular dynamics technique along 50 ns of simulation time. Therefore, L28 and L30 drugs could be safely and securely applicable as therapeutics in medicine to enhance human memory performance.

Author contribution statement

Mohamed El fadili: Conceived and designed the experiments; Performed the experiments; Contributed reagents, materials, analysis tools or data; Wrote the paper.

Mohammed Er-rajy: Conceived and designed the experiments; Contributed reagents, and analysis tools.

Hamada Imtara: Analyzed and interpreted the data; Contributed reagents; Wrote the paper.

Omar M. Noman, Ramzi A Mothana: Analyzed and interpreted the data; Wrote the paper.

Sheaf Abdullah, Sara Zerougui: Analyzed and interpreted the data.

Menana Elhallaoui: Conceived and designed the experiments.

Data availability statement

Data included in article/supplementary material/referenced in article.

Declaration of interest's statement

The authors declare that they have no known competing financial interests or personal relationships that could have appeared to influence the work reported in this paper.

Additional information

Supplementary content related to this article has been published online at [URL].

Appendix A. Supplementary data

Supplementary data to this article can be found online at https://doi.org/10.1016/j.heliyon.2023.e13706.

References

[1] N. Nazir, M. Nisar, M. Zahoor, F. Uddin, S. Ullah, R. Ullah, S.A. Ansari, H.M. Mahmood, A. Bari, A. Alobaid, Phytochemical analysis, in vitro anticholinesterase, antioxidant activity and in vivo nootropic effect of Ferula ammoniacum (dorema ammoniacum) D. Don. In scopolamine-induced memory impairment in mice, Brain Sci. 11 (2021) 259, https://doi.org/10.3390/brainsci11020259.
[2] B. Couto, G. Rojas, C. Gelormini-Lezama, S. O'Neill, Memory, executive function and social cognition in neurological disorders, in: Encyclopedia of Behavioral Neuroscience, second ed., Elsevier, 2022, pp. 140–147, https://doi.org/10.1016/B978-0-12-819641-0.00032-3.
[3] V.J. Santora, T.A. Almos, R. Barido, J. Basinger, C.L. Bellows, B.C. Bookser, J.G. Breitenbucher, N.J. Broadbent, C. Cabebe, C.-K. Chai, M. Chen, S. Chow, D. M. Chung, L. Crickard, A.M. Danks, G.C. Freestone, D. Gitnick, V. Gupta, C. Hoffmaster, A.R. Hudson, A.P. Kaplan, M.R. Kennedy, D. Lee, J. Limberis, K. Ly, C. C. Mak, B. Masatsugu, A.C. Morse, J. Na, D. Neul, J. Nikpur, M. Peters, R.E. Petroski, J. Renick, K. Sebring, S. Sevidal, A. Tabatabaei, J. Wen, Y. Yan, Z.W. Yoder, D. Zook, Design and synthesis of novel and selective Glycine transporter-1 (GlyT1) inhibitors with memory enhancing properties, J. Med. Chem. 61 (2018) 6018–6033, https://doi.org/10.1021/acs.jmedchem.8b00372.
[4] V. Eulenburg, W. Armsen, H. Betz, J. Gomeza, Glycine transporters: essential regulators of neurotransmission, Trends Biochem. Sci. 30 (2005) 325–333, https://doi.org/10.1016/j.tibs.2005.04.004.
[5] A.R. Hudson, V.J. Santora, R.E. Petroski, T.A. Almos, G. Anderson, R. Barido, J. Basinger, C.L. Bellows, B.C. Bookser, N.J. Broadbent, C. Cabebe, C.-K. Chai, M. Chen, S. Chow, D.M. Chung, L. Heger, A.M. Danks, G.C. Freestone, D. Gitnick, V. Gupta, C. Hoffmaster, A.P. Kaplan, M.R. Kennedy, D. Lee, J. Limberis, K. Ly, C.C. Mak, B. Masatsugu, A.C. Morse, J. Na, D. Neul, J. Nikpur, J. Renick, K. Sebring, S. Sevidal, A. Tabatabaei, J. Wen, S. Xia, Y. Yan, Z.W. Yoder, D. Zook, M. Peters, J.G. Breitenbucher, Azetidine-based selective glycine transporter-1 (GlyT1) inhibitors with memory enhancing properties, Bioorg. Med. Chem. Lett 30 (2020), 127214, https://doi.org/10.1016/j.bmcl.2020.127214.
[6] M. El fadili, M. Er-Rajy, M. Kara, A. Assouguem, A. Belhassan, A. Alotaibi, N.N. Mrabti, H. Fidan, R. Ullah, S. Ercisli, S. Zarougui, M. Elhallaoui, QSAR, ADMET in silico pharmacokinetics, molecular docking and molecular dynamics studies of novel bicyclo (aryl methyl) benzamides as potent GlyT1 inhibitors for the treatment of schizophrenia, Pharmaceuticals 15 (2022) 670, https://doi.org/10.3390/ph15060670.
[7] M. Radan, T. Djikic, D. Obradovic, K. Nikolic, Application of in vitro PAMPA technique and in silico computational methods for blood-brain barrier permeability prediction of novel CNS drug candidates, Eur. J. Pharmaceut. Sci. 168 (2022), 106056, https://doi.org/10.1016/j.ejps.2021.106056.
[8] S. Vilar, G. Cozza, S. Moro, Medicinal chemistry and the molecular operating environment (MOE): application of QSAR and molecular docking to drug discovery, Curr. Top. Med. Chem. 8 (2008) 1555–1572, https://doi.org/10.2174/156802608786786624.
[9] O. Ebenezer, N. Damoyi, M.A. Jordaan, M. Shapi, Unveiling of pyrimidindinones as potential anti-norovirus agents—a pharmacoinformatic-based approach, Molecules 27 (2022) 380, https://doi.org/10.3390/molecules27020380.
[10] S. Tian, J. Wang, Y. Li, D. Li, L. Xu, T. Hou, The application of in silico drug-likeness predictions in pharmaceutical research, Adv. Drug Deliv. Rev. 86 (2015) 2–10, https://doi.org/10.1016/j.addr.2015.01.009.
[11] A. Serrano, B. Imbernón, H. Pérez-Sánchez, J.M. Cecilia, A. Bueno-Crespo, J.L. Abellán, Qn-Docking, An innovative molecular docking methodology based on Q-Networks, Appl. Soft Comput. 96 (2020), 106678, https://doi.org/10.1016/j.asoc.2020.106678.
[12] R.P.D. Bank, RCSB PDB - 4M48: X-ray structure of dopamine transporter elucidates antidepressant mechanism, (n.d.). https://www.rcsb.org/structure/4M48 (accessed July 4, 2022).
[13] E. Wang, H. Sun, J. Wang, Z. Wang, H. Liu, J.Z.H. Zhang, T. Hou, End-point binding free energy calculation with MM/PBSA and MM/GBSA: strategies and applications in drug design, Chem. Rev. 119 (2019) 9478–9508, https://doi.org/10.1021/acs.chemrev.9b00055.
[14] T.A. de Oliveira, L.R. Medaglia, E.H.B. Maia, L.C. Assis, P.B. de Carvalho, A.M. da Silva, A.G. Taranto, Evaluation of docking machine learning and molecular dynamics methodologies for DNA-ligand systems, Pharmaceuticals 15 (2022) 132, https://doi.org/10.3390/ph15020132.
[15] Gaussian 09 Citation | Gaussian.com, (n.d.). https://gaussian.com/g09citation/ (accessed July 6, 2022).
[16] R.G. Parr, Density functional theory of atoms and molecules, in: K. Fukui, B. Pullman (Eds.), Horizons of Quantum Chemistry, Springer Netherlands, Dordrecht, 1980, pp. 5–15, https://doi.org/10.1007/978-94-009-9027-2_2.
[17] H. Wang, Y. Jia, G. Jing, X. Wu, A novel toxicity prediction model for hydrazine compounds based on 1D–3D molecular descriptors, Computational Toxicology 18 (2021), 100169, https://doi.org/10.1016/j.comtox.2021.100169.
[18] G.W.A. Milne, Software review of ChemBioDraw 12.0, J. Chem. Inf. Model. 50 (2010) 2053, https://doi.org/10.1021/ci100385n.
[19] T. Österberg, U. Norinder, Prediction of drug transport processes using simple parameters and PLS statistics the use of ACD/logP and ACD/ChemSketch descriptors, Eur. J. Pharmaceut. Sci. 12 (2001) 327–337, https://doi.org/10.1016/S0928-0987(00)00189-5.
[20] C. Guerra Tort, V. Aguiar Pulido, V. Suárez Ulloa, F. Docampo Boedo, J.M. López Gestal, J. Pereira Loureiro, Electronic Health records exploitation using artificial intelligence techniques, in: 3rd XoveTIC Conference, MDPI, 2020, p. 60, https://doi.org/10.3390/proceedings2020054060.
[21] Introducing the XLSTAT Free edition, XLSTAT, Your data analysis solution. (n.d.). https://www.xlstat.com/en/news/introducing-the-xlstat-free-edition (accessed March 8, 2022).
[22] N. Mostoufi, A. Constantinides, Chapter 8 - linear and nonlinear regression analysis, in: N. Mostoufi, A. Constantinides (Eds.), Applied Numerical Methods for Chemical Engineers, Academic Press, 2023, pp. 403–476, https://doi.org/10.1016/B978-0-12-822961-3.00008-X.
[23] A.K. Halder, T. Jha, Validated predictive QSAR modeling of N-aryl-oxazolidinone-5-carboxamides for anti-HIV protease activity, Bioorg. Med. Chem. Lett 20 (2010) 6082–6087, https://doi.org/10.1016/j.bmcl.2010.08.050.
[24] K. Roy, S. Kar, R.N. Das, Validation of QSAR models, in: Understanding the Basics of QSAR for Applications in Pharmaceutical Sciences and Risk Assessment, Elsevier, 2015, pp. 231–289, https://doi.org/10.1016/B978-0-12-801505-6.00007-7.
[25] C.A. Lipinski, F. Lombardo, B.W. Dominy, P.J. Feeney, Experimental and computational approaches to estimate solubility and permeability in drug discovery and development settings, Adv. Drug Deliv. Rev. 23 (1997) 3–25, https://doi.org/10.1016/S0169-409X(96)00423-1.
[26] D.F. Veber, S.R. Johnson, H.-Y. Cheng, B.R. Smith, K.W. Ward, K.D. Kopple, Molecular properties that influence the oral bioavailability of drug candidates, J. Med. Chem. 45 (2002) 2615–2623, https://doi.org/10.1021/jm020017n.
[27] W.J. Egan, M. Merz Kenneth, J.J. Baldwin, Prediction of drug absorption using multivariate statistics, J. Med. Chem. 43 (2000) 3867–3877, https://doi.org/10.1021/jm000292e.
[28] W.J. Egan, G. Lauri, Prediction of intestinal permeability, Adv. Drug Deliv. Rev. 54 (2002) 273–289, https://doi.org/10.1016/S0169-409X(02)00004-2.
[29] S. Yalcin, Molecular docking, drug likeness, and ADMET analyses of passiflora compounds as P-glycoprotein (P-gp) inhibitor for the treatment of cancer, Current Pharmacology Reports 6 (2020) 429–440, https://doi.org/10.1007/s40495-020-00241-6.
[30] I. Muegge, S.L. Heald, D. Brittelli, Simple selection criteria for drug-like chemical matter, J. Med. Chem. 44 (2001) 1841–1846, https://doi.org/10.1021/jm015507e.
[31] (n.d. pkCSM. http://biosig.unimelb.edu.au/pkcsm/run_example?. (Accessed 6 July 2022) accessed.
[32] A. Daina, O. Michielin, V. Zoete, SwissADME: a free web tool to evaluate pharmacokinetics, drug-likeness and medicinal chemistry friendliness of small molecules, Sci. Rep. 7 (2017), 42717, https://doi.org/10.1038/srep42717.

[33] D. Bassani, M. Pavan, G. Bolcato, M. Sturlese, S. Moro, Re-exploring the ability of common docking programs to correctly reproduce the binding modes of non-covalent inhibitors of SARS-CoV-2 protease mpro, Pharmaceuticals 15 (2022) 180, https://doi.org/10.3390/ph15020180.

[34] R.P.D. Bank, RCSB PDB - 4M48: X-ray structure of dopamine transporter elucidates antidepressant mechanism, (n.d.). https://www.rcsb.org/structure/4M48 (accessed August 23, 2022).

[35] A. Kouranov, The RCSB PDB information portal for structural genomics, Nucleic Acids Res. 34 (2006), https://doi.org/10.1093/nar/gkj120. D302–D305.

[36] BIOVIA Discovery Studio - BIOVIA - Dassault Systèmes®, (n.d.). https://www.3ds.com/products-services/biovia/products/molecular-modeling-simulation/biovia-discovery-studio/(accessed August 23, 2022).

[37] M. El fadili, M. Er-rajy, H. Imtara, M. Kara, S. Zarougui, N. Altwaijry, O. Al kamaly, A. Al Sfouk, M. Elhallaoui, 3D-QSAR, ADME-tox in silico prediction and molecular docking studies for modeling the analgesic activity against neuropathic pain of novel NR2B-selective NMDA receptor antagonists, Processes 10 (2022) 1462, https://doi.org/10.3390/pr10081462.

[38] A.P. Norgan, P.K. Coffman, J.-P.A. Kocher, D.J. Katzmann, C.P. Sosa, Multilevel parallelization of AutoDock 4.2, J. Cheminf. 3 (2011) 12, https://doi.org/10.1186/1758-2946-3-12.

[39] Desmond | Schrodinger, (n.d.). https://www.schrodinger.com/products/desmond (accessed April 28, 2022).

[40] G.A. Kaminski, R.A. Friesner, J. Tirado-Rives, W.L. Jorgensen, Evaluation and reparametrization of the OPLS-AA force field for proteins via comparison with accurate quantum chemical calculations on peptides, J. Phys. Chem. B 105 (2001) 6474–6487, https://doi.org/10.1021/jp003919d.

[41] E. Wang, H. Sun, J. Wang, Z. Wang, H. Liu, J.Z.H. Zhang, T. Hou, End-point binding free energy calculation with MM/PBSA and MM/GBSA: strategies and applications in drug design, Chem. Rev. 119 (2019) 9478–9508, https://doi.org/10.1021/acs.chemrev.9b00055.

[42] A. Bastianoni, E. Guastaldi, A. Barbagli, S. Bernardinetti, A. Zirulia, M. Brancale, T. Colonna, Multivariate analysis applied to aquifer hydrogeochemical evaluation: a case study in the coastal significant subterranean water body between "cecina river and san vincenzo", Tuscany (Italy), Applied Sciences 11 (2021) 7595, https://doi.org/10.3390/app11167595.

[43] M. Er-rajy, M. El Fadili, H. Hadni, N.N. Mrabti, S. Zarougui, M. Elhallaoui, 2D-QSAR modeling, drug-likeness studies, ADMET prediction, and molecular docking for anti-lung cancer activity of 3-substituted-5-(phenylamino) indolone derivatives, Struct. Chem. 33 (2022) 973–986, https://doi.org/10.1007/s11224-022-01913-3.

[44] G.K. Uyanık, N. Güler, A study on multiple linear regression analysis, Procedia - Social and Behavioral Sciences 106 (2013) 234–240, https://doi.org/10.1016/j.sbspro.2013.12.027.

[45] N. Kravić, J. Savosina, M. Agafonova-Moroz, V. Babain, A. Legin, D. Kirsanov, Nonlinear multivariate regression algorithms for improving precision of multisensor potentiometry in analysis of spent nuclear fuel reprocessing solutions, Chemosensors 10 (2022) 90, https://doi.org/10.3390/chemosensors10030090.

[46] R. Kasmi, E. Hadaji, O. Chedadi, A. El Aissouq, M. Bouachrine, A. Ouammou, 2D-QSAR and docking study of a series of coumarin derivatives as inhibitors of CDK (anticancer activity) with an application of the molecular docking method, Heliyon 6 (2020), e04514, https://doi.org/10.1016/j.heliyon.2020.e04514.

[47] E. Pourbasheer, S. Riahi, M.R. Ganjali, P. Norouzi, Quantitative structure–activity relationship (QSAR) study of interleukin-1 receptor associated kinase 4 (IRAK-4) inhibitor activity by the genetic algorithm and multiple linear regression (GA-MLR) method, J. Enzym. Inhib. Med. Chem. 25 (2010) 844–853, https://doi.org/10.3109/14756361003757893.

[48] M. Er-rajy, M. El fadili, N.N. Mrabti, S. Zarougui, M. Elhallaoui, QSAR, Molecular docking, ADMET properties in silico studies for a series of 7-propanamide benzoxaboroles as potent anti-cancer Agents, Chin. J. Anal. Chem. (2022), 100163, https://doi.org/10.1016/j.cjac.2022.100163.

[49] K.B. de C. Rezende, A.J.L.A. da Cunha, J. Amim Junior, R.G. Bornia, External validation of the Fetal Medicine Foundation algorithm for the prediction of preeclampsia in a Brazilian population, Pregnancy Hypertension 17 (2019) 64–68, https://doi.org/10.1016/j.preghy.2019.05.006.

[50] M. Rafało, Cross Validation Methods: Analysis Based on Diagnostics of Thyroid Cancer Metastasis, ICT Express, 2021, https://doi.org/10.1016/j.icte.2021.05.001. S2405959521000552.

[51] A. Golbraikh, A. Tropsha, Beware of q2, J. Mol. Graph. Model. 20 (2002) 269–276, https://doi.org/10.1016/S1093-3263(01)00123-1.

[52] A. Daina, V. Zoete, A BOILED-egg to predict gastrointestinal absorption and brain penetration of small molecules, ChemMedChem 11 (2016) 1117–1121, https://doi.org/10.1002/cmdc.201600182.

[53] C.-Y. Jia, J.-Y. Li, G.-F. Hao, G.-F. Yang, A drug-likeness toolbox facilitates ADMET study in drug discovery, Drug Discov. Today 25 (2020) 248–258, https://doi.org/10.1016/j.drudis.2019.10.014.

[54] A. Adamski, D. Kruszka, Z. Dutkiewicz, M. Kubicki, A. Gorczyński, V. Patroniak, Novel family of fused tricyclic [1,4]diazepines: design, synthesis, crystal structures and molecular docking studies, Tetrahedron 73 (2017) 3377–3386, https://doi.org/10.1016/j.tet.2017.05.015.

[55] A. Penmatsa, K.H. Wang, E. Gouaux, X-ray structure of dopamine transporter elucidates antidepressant mechanism, Nature 503 (2013) 85–90, https://doi.org/10.1038/nature12533.

[56] A. Belhassan, H. Zaki, M. Benlyas, T. Lakhlifi, M. Bouachrine, Study of novel triazolo-benzodiazepine analogues as antidepressants targeting by molecular docking and ADMET properties prediction, Heliyon 5 (2019), e02446, https://doi.org/10.1016/j.heliyon.2019.e02446.

[57] Zentrum für Bioinformatik: Universität Hamburg - Proteins Plus Server, (n.d.). https://proteins.plus/(accessed August 29, 2022).

[58] M. Abdullahi, G.A. Shallangwa, A. Uzairu, In silico QSAR and molecular docking simulation of some novel aryl sulfonamide derivatives as inhibitors of H5N1 influenza A virus subtype, Beni-Suef Univ J Basic Appl Sci. 9 (2020) 2, https://doi.org/10.1186/s43088-019-0023-y.